Ceramics International 43 (2017) 14659–14665

Contents lists available at ScienceDirect

Ceramics International

journal homepage: www.elsevier.com/locate/ceramint

Influence of micro- and nanoparticles of zirconium oxides on the dielectric properties of $CaCu_3Ti_4O_{12}$

Rodrigo Espinoza-González*, Edgar. Mosquera**,[1]

Departamento de Ciencia de los Materiales, FCFM, Universidad de Chile, Av. Beauchef 851, 8370456 Santiago, Chile

ARTICLE INFO

Keywords:
Dielectric ceramics
Doped CCTO
Impedance spectroscopy
IBLC

ABSTRACT

This work presents the results of Zr oxide doping of a $CaCu_3Ti_4O_{12}$ (CCTO) ceramic prepared by a solid-state reaction. Different stoichiometries (ZrO and ZrO_2) and grain sizes (micro- and nanoparticles) were added as dopants at concentrations of 0.5 and 1.0 wt%. Zr-doping controls the grain size growth, leading to a reduction of the grain size as observed by scanning electron microscopy. For both dopant concentrations, all of the samples exhibited lower dielectric loss and a smaller dielectric constant than those of undoped CCTO. The sample doped with 0.5% of the non-stoichiometric ZrO exhibits a dielectric constant over 3200 and a dissipation factor of 0.02 at 1 kHz. The impedance spectroscopy analysis confirms that the decrease of dielectric loss is mainly due to an increase in resistivity at grain boundaries, which is attributed to the suppression of oxygen-loss promoted by dopants.

1. Introduction

In recent years, the $CaCu_3Ti_4O_{12}$ (CCTO) compound has attracted a much attention due to its extremely high dielectric constant (up to 10.000 at 1 kHz) [1,2]. The dielectric constant of CCTO is almost temperature independent over a broad range of temperatures extending from 100 to 600 K and over a rather wide microwave frequency window [3]. Such unique properties of the material are very promising for capacitor applications and certainly for microelectronics and microwave devices (mobile cell phones, for example) [4].

Despite the origin of the promising properties of CCTO not yet being well-understood [5], the most widely accepted model is attributed to an internal barrier layer capacitance (IBLC) effect originating from extrinsic polarization at the grain boundaries. In this model, bulk grains have a semiconductive behavior, and grain boundaries have high resistance. According to the IBLC model, dielectric loss is closely correlated with insulation of the barrier layer. Commonly, high resistance of the barrier layer corresponds to low conductance, which means low tanδ. The addition of dopants seems to be an effective method to control the chemistry and structure of interfacial regions at grain boundaries, which increases the barrier layer resistance and decreases the dielectric loss.

The effect of several additives as dopants has been extensively studied with the aim of decreasing the dielectric loss (tan(δ)) of CCTO. For example, Cr, Mn, Co, Ni, Nb [6–17], Zr [18–24], Zn [25,26], Sr [27–29] and Sc [30] have been used to decrease tan(δ) by controlling the chemistry and structure of interfacial regions at grain boundaries. Recently, co-doping has also been used to simultaneously suppress grain growth and enhance grain boundary resistivity for reducing the dielectric loss. In this sense, Thomas et al. [31] doping CCTO with La/Nb had a significant impact on the dielectric properties, and Boonlakhorn et al. [32] reported promising results using a combination of Y/Mg as dopants.

Among these mentioned reports, Zr doping has been shown to both reduce tan(δ) and the dielectric constant prepared by different routes. Kwon et al. [20] reported the results of CCTO doped with 0.5 wt% of ZrO_2 prepared by a solid-state reaction; they obtained a dielectric constant of approximately 5600 and tan(δ) of 0.5 at 1 kHz. Patterson et al. [18] reported a similar dielectric constant but smaller tan(δ) of 0.016 at 1 kHz for 0.1 wt% of ZrO_2 prepared by the same route. The same method was also used by Thongbai et al. [24] to obtain a minimum tan(δ) of 0.038 at 2 kHz and a permittivity of 4610. The sol-gel route was used by Chi et al. [22] and reported a tanδ of 0.075 at 60 kHz with a dielectric constant below 10,000, whereas Sun et al. [23] obtained a tan(δ) of 0.026 at 10 kHz and a permittivity of approximately 25,000, above the permittivity of undoped CCTO, in Zr-doped CCTO prepared by the same method.

The scope of this work is to study the influence of both the particle size and stoichiometric composition of the zirconium oxide used as a dopant

* Corresponding author.
** Departamento de Física, Universidad del Valle, A.A. 25360, Cali, Colombia.
E-mail address: roespino@ing.uchile.cl (R. Espinoza-González).
[1] Present address: Departamento de Física, Universidad del Valle, A.A. 25360, Cali, Colombia.

http://dx.doi.org/10.1016/j.ceramint.2017.07.183
Received 16 June 2017; Received in revised form 25 July 2017; Accepted 26 July 2017
Available online 27 July 2017

agent on the CCTO dielectric properties prepared by a solid-state reaction.

2. Experimental procedure

The CCTO compound was prepared by a conventional solid-state reaction route using the following high purity starting materials from Sigma-Aldrich: $CaCO_3$ (> 99%), CuO (99.99%) and anatase-TiO_2 (99.8%). Three different zirconium oxide dopants were added at concentrations of 0.5 and 1.0 wt%: a) micrometric m-ZrO_2 (99% pure, 5 μm average size, monoclinic phase; Aldrich), b) micrometric ZrO (99.3%; Lab. Balzers), and c) nanometric n-ZrO_2 (99%, 15–25 nm average powder size; Alfa-Aesar). Stoichiometric amounts of precursor powders were weighed and mixed with the proper amount of dopants in an agate mortar over 1 h and then calcined at 950 °C for 24 h. Calcined powders were pressed at 500 MPa into pellets 9 mm in diameter with 1 mm thickness and later sintered in air at 1050 °C over 12 h. For the sake of clarity, the samples were named 0.5mZO_2, 0.5ZO and 0.5nZO2 for the 0.5 wt% dopant concentration and 1.0mZO2, 1.0ZO and 1.0nZO2 for the 1.0 wt% dopant concentration.

Sintered pellets were characterized by X-ray diffraction (XRD) in a Bruker D8 diffractometer using Cu $K\alpha_{1,2}$ radiation. The data were collected at room temperature with a step size and scan rate of 0.01° and 0.1 s, respectively. The X-ray tube was operated at 40 kV and 30 mA. Rietveld refinement of XRD patterns was performed using TOPAS software for which a pseudo-Voigt function was chosen as a profile function. The final density of the sintered pellets was measured by the Archimedes method. The microstructure and composition of the pellets were studied in a scanning electron microscope (SEM; FEI Quanta 250), and the different zirconium oxides were characterized by SEM and transmission electron microscopy (TEM) using an FEI Tecnai F20. Raman spectra were recorded at room temperature in a back-scattering geometry using a WITec alpha300R spectrometer (model CRC200). Radiation of 633 nm (1.96 eV) from a He-Ne laser was focused on the sample using a 100X objective. For impedance measurements, gold electrodes were sputtered over a polished surface of sintered samples. Impedance measurements were performed in the frequency range between 0.1 Hz and 1 MHz with an applied voltage of 1 V in a Princeton Applied Research impedance analyzer (model VersaSTAT 4). Impedance measurements at temperatures ranging from 300 to 385 K were performed using an Instek LCR meter (model 8101 G) in the frequency range of 20 Hz to 1 MHz.

2.1. Characterization of zirconium oxides

The size and composition of the zirconium oxides used to prepare the different doped CCTO ceramics was verified by electron microscopy. Panels (a) and (b) in Fig. 1 show SEM images of m-ZrO_2 and ZrO powders, respectively. The micrometric sizes of both oxide particles confirm an average particle size of 5 μm for m-ZrO_2 and 4 μm for ZrO powders. n-ZrO_2 was characterized by TEM as shown in Fig. 1(c), which also verifies the nanoscale particle size of the powders informed by the supplier.

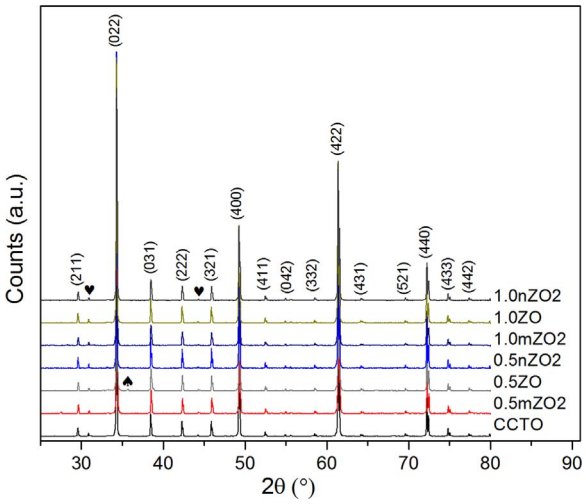

Fig. 2. XRD patterns of pure and Zr-oxide-doped CCTO samples. ([a]) Peak of CuO (002) reflection. (♥) Peaks of K_β reflection of (022) and (321) planes.

The oxidation states of zirconium are (0) and (IV); thus, the initial ZrO dopant powders were characterized to elucidate its actual composition. The ZrO powders were ground in an agate mortar and analyzed by XRD. The best Rietveld refinement, with a Good of Fitness value (GoF) of 1.53, is provided by the combination of monoclinic ZrO_2 (58.4 wt%) and hexagonal $ZrO_{0.27}$ (41.6 wt%), which led to a Zr:O ratio of 1:1.3, roughly the average stoichiometry of ZrO.

3. Results and discussion

3.1. X-ray analysis

Fig. 2 shows the XRD patterns of pure and Zr-doped CCTO samples after sintering. XRD analysis confirms the single-phase formation of the pseudo-cubic CCTO compound by comparing with the standard powder diffraction file database (JCPDF File No. 75-1149) with no traces of Zr-oxide compounds. Rietveld refinement also confirmed single-phase formation of CCTO for all of the samples and a small amount of 0.3 wt% of CuO in the 0.5ZO sample. The unit cell parameter (a_0, nm) of undoped sample determined by Rietveld analysis is 0.7395 nm, which is similar to the values obtained for all doped ceramics (see Table 1), with a GoF parameter between 1.4 and 1.6, indicating the reliability of refined structural parameters. The slight variations of a_0 between pure and doped CCTO seems to indicate that Zr is not incorporated into the crystalline structure and that most of the dopants would be present in the microstructure either in the grain boundaries or as a second phase not detectable by XRD since they are

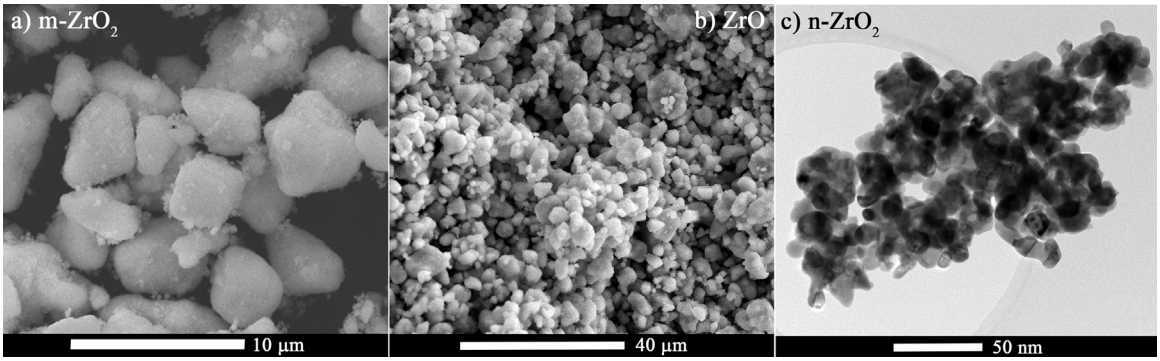

Fig. 1. Electron microscopy images of the different zirconium oxides used as dopants: (a) m-ZrO_2, (b) ZrO and (c) n-ZrO_2.

Table 1
Lattice parameter (a_0) determined by Rietveld refinement, density and average grain size (D).

Material	a_0 (nm)	*Density* (g/cm^3)	D (μm)
CCTO	0.7395	4.68	4.7
0.5ZO	0.7394	4.54	3.6
0.5mZO2	0.7394	4.67	3.3
0.5nZO2	0.7394	4.78	2.4
1.0ZO	0.7395	4.63	3.1
1.0mZO2	0.7396	4.53	2.5
1.0nZO2	0.7395	4.62	3.8

below the typical detection limit of this technique. The relative density of all the samples measured by the Archimedes method is also included in Table 1. All the values are over 90% of the theoretical value for CCTO and are similar to results reported for doped CCTO [14,21,25,28,33].

3.2. SEM analysis

The SEM images of doped CCTO samples are displayed in Fig. 3, where it can be seen that the microstructure is influenced by the different dopants and concentrations through changes in the grain size. The average grain size (D, μm) measured from SEM images is included in Table 1. The grain size of all doped compounds is smaller than the grain size of undoped CCTO (image not shown) in which two different tendencies are observed depending on the grain size of the dopant. Micrometric dopants (m-ZrO2 and ZrO) tend to decrease D with increasing amount of dopant. Thus, the average grain size of sample 0.5ZO is 3.6 μm and that of 1.0ZO is 3.1 μm, and a similar tendency is observed for samples 0.5ZO2 and 1.0ZO2. Decreasing grain size with Zr doping was also previously reported in different studies [22,23,34], which suggests that Zr doping plays a role in controlling the grain size growth during the sintering process. In contrast, samples doped with nanometric n-ZrO_2 exhibited an increase of D from 2.4 to 3.8 μm upon incrementing the dopant concentration.

EDS analyses reveals the stoichiometric relationship between Ca, Cu and Ti that corresponds to CCTO ceramics for all of the samples and confirms the presence of Zr in amounts close to the expected values. Fig. 4(a) shows EDS spectra obtained on the surface of the 0.5ZO sample from grains of the smooth surface indicated by CCTO+Zr arrows in Fig. 3(a). This sample also has roughness grains that correspond to grains of CuO as revealed by EDS (see Fig. 4(b)). This confirms the presence of CuO detected by XRD. Considering that the SEM beam spot is bigger than the CuO grain analyzed, the small Ti peak in this spectrum could be produced by one of the neighboring grains.

3.3. Raman spectroscopy

Fig. 5 displays the Raman spectra of pure and doped CCTO sintered samples. Four evident peaks are present for all of the samples, which are in good agreement with values of Raman modes reported in the literature [35,36] with deviations of less than 5 cm^{-1}. The two main peaks present at 449 and 513 cm^{-1} are assigned to Ag-symmetry (TiO_6) rotation-like lattice vibrations, while the Raman line at 579 cm^{-1} is associated with Fg-symmetry (O-Ti-O) anti-stretching mode. Another line at 288 cm^{-1} is a weak low frequency peak associated with Fg-symmetry (TiO_6) rotation-like vibration mode. Raman lines related to Zr oxides were absent of the spectra, which can be attributed to undetectable signals due to the small amounts added to the ceramic compounds. The slight deviations of the Raman lines are common to all doped and undoped samples, suggesting that the addition of Zr oxides does not visibly affect the frequency of vibrational modes.

Nevertheless, similar to Li et al. [34], the major difference observed in the Raman spectra is the intensity reduction of the Ag bands that was related by those authors to a lower rotation of the octahedron associated with this band. A slight reduction of Fg is also observed in Fig. 5, which could be caused by the off-center displacement of Ti ions within the TiO_6 octahedron [34]. It is worth noting that the reduction in intensity is less strong in the 0.5nZO2 sample.

3.4. Dielectric properties

The dielectric constant (ε') and dielectric loss (tan(δ)) of Zr-doped and undoped CCTO measured at room temperature are plotted as a function of the frequency in Fig. 6. The values of pure CCTO are in

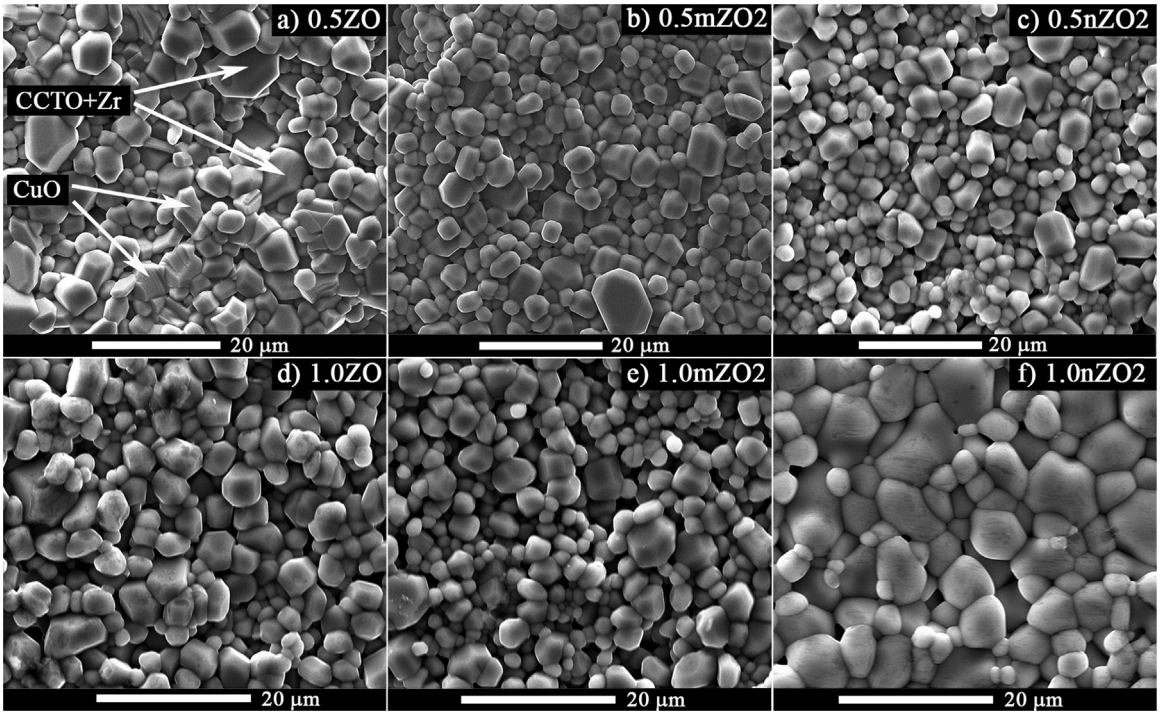

Fig. 3. SEM images of the different Zr-oxide-doped CCTO ceramics: (top row) 0.5 wt% of dopant, (bottom row) 1.0 wt% of dopant.

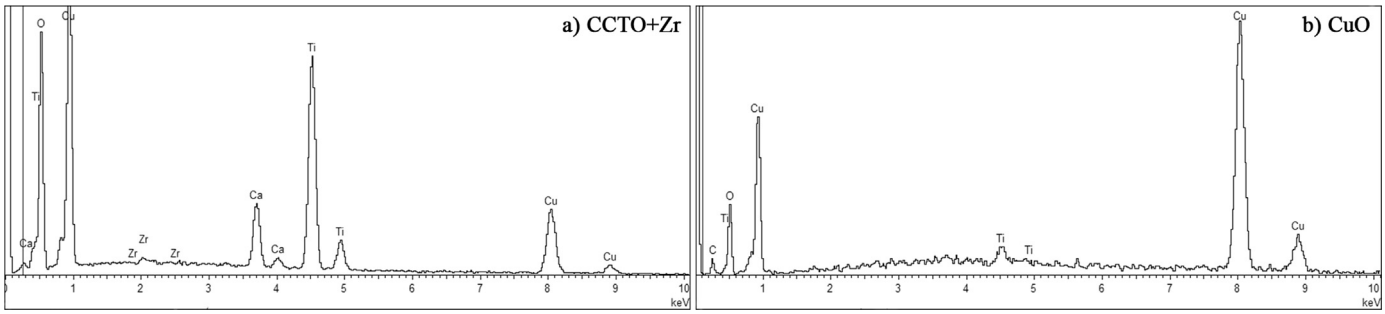

Fig. 4. EDS spectra detected on the surface of the 0.5ZO sample: spectra of (a) Zr-doped CCTO and (b) CuO grains.

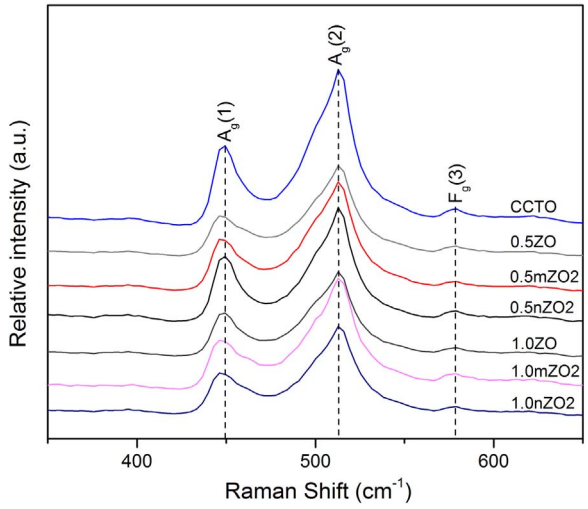

Fig. 5. Raman spectra of pure and Zr-oxide-doped CCTO samples.

agreement with those reported in the literature [1,2] for which ε' decreases by increasing the frequency in two stages steeply at approximately 10 Hz, which has been related to a sample-electrode interface effect [30]. The doped ceramics with 0.5 wt% of micro- and nano-ZrO_2 reduces ε' over the entire frequency range compared to that of undoped CCTO, having higher reduction for the 0.5nZO2 sample (see Fig. 6(a)). ZrO additive reduces ε' for frequencies lower than 200 kHz, leading to ε' that remains nearly constant (in the range from 3800 to 2800) at frequencies higher than 100 Hz.

The increase of dopant up to 1 wt% produces a slight decrease of the dielectric constant in sample 1.0ZO (Fig. 6(b)), whereas in sample 1.0ZO2, it leads to a noticeable increase of ε' below 100 Hz, similar to the behavior of undoped CCTO, but remains nearly independent of the frequency over 100 Hz. It is worth noting that the nano-ZrO_2 dopant exhibits a noticeable increase in the dielectric constant by increasing the concentration of the dopant from 0.5 to 1 wt%.

Fig. 6(c) shows that the dielectric loss of the whole set of CCTO samples with a 0.5 wt% dopant concentration is lower than that of pure CCTO. The lowest tan(δ) is for the 0.5ZO sample, which presents values below 0.021 between 0.1 and 1 kHz, which is lower than most of the previously reported results of Zr-doped CCTO [18–24]. Undoped

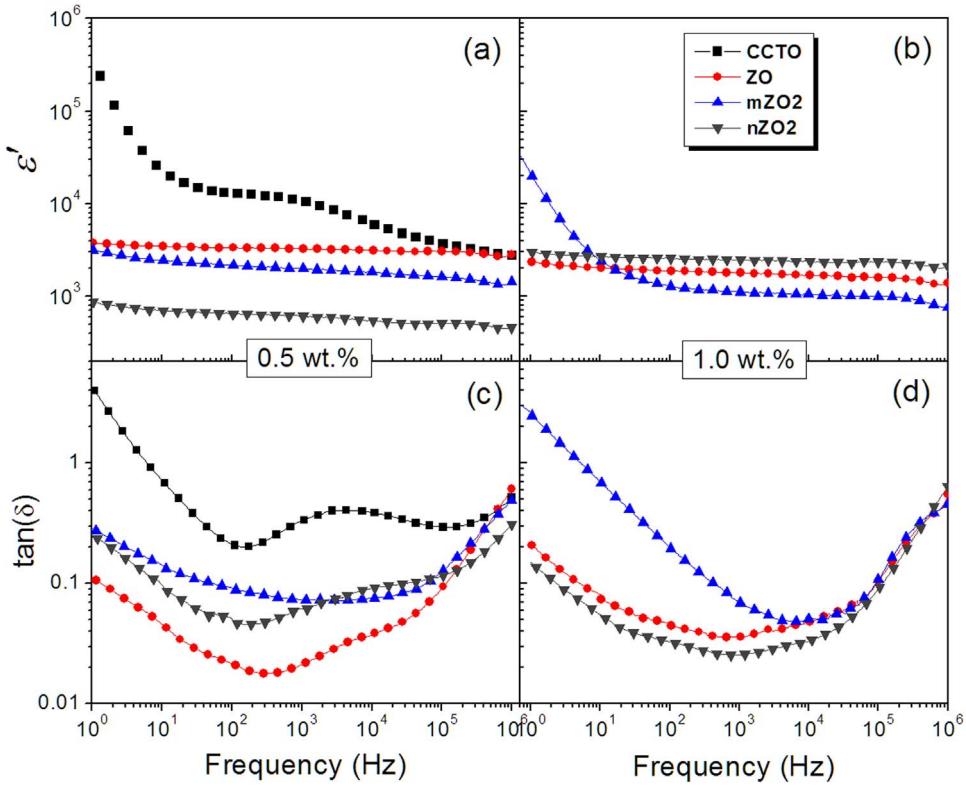

Fig. 6. Dielectric constant (ε') and dielectric loss (tan(δ)) of Zr-doped and undoped CCTO ceramics.

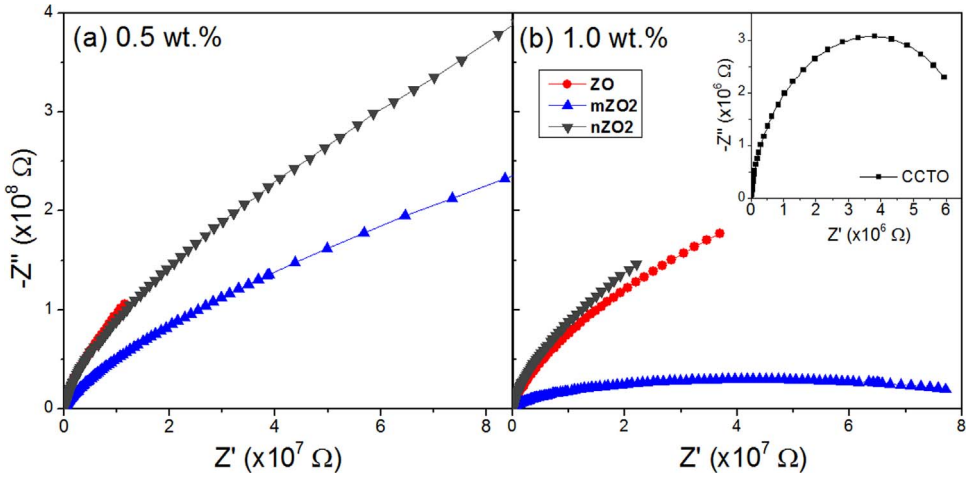

Fig. 7. Complex impedance plane plots of Zr-doped and undoped CCTO ceramics (inset (b)).

Table 2
Bulk grain (R_b) and grain boundary (R_{gb}) resistivity from fitted impedance curves and activation energies for bulk and grain boundary RC elements.

Material	R_b (Ω cm)	R_{gb} (MΩ cm)	$E_{a,gb}$ (meV)	$E_{a,gb}$ (meV)
CCTO	58.3	21.9	53	683
0.5ZO	67.3	8239.6	137	923
0.5mZO2	167.4	273.7	103	726
0.5nZO2	164.4	14,608.0	83	434
1.0ZO	156.0	4734.9	118	891
1.0mZO2	253.2	390.7	125	837
1.0nZO2	172.6	6652.6	146	936

CCTO exhibits a relaxation peak between 1 and 10 kHz that is modestly present in 0.5ZO and 0.5nZO2 samples but is not present in the other doped samples. On the other hand, it is interesting to note that, among the samples doped with 1.0 wt%, the 1.0nZO2 sample presents the lowest tan(δ) (see Fig. 6(d)) over the whole frequency range.

Fig. 7 shows the complex (Z*) impedance plane plots for undoped and Zr-doped CCTO. The inset in Fig. 6(b) corresponds to the complex impedance of undoped CCTO, which is an order of magnitude smaller than that of doped CCTO ceramics, similar to the results reported by Chi *et al.* [22]. For both concentrations, the CCTO samples doped with ZrO and n-ZrO_2 exhibited bigger semi-circular arcs than the samples doped with m-ZrO_2. The impedance behavior of CCTO compounds can be modeled as an equivalent circuit that consists of two parallel RC elements connected in series, where each RC element represents the grain bulk and grain boundary effects [21,23]. The representation of this model means that the nonzero intercept at high frequency represents the resistance of grains (R_b) [12], and the curve fit of the impedance complex plot allows for extrapolating the curve intercept to estimate the grain boundary resistance (R_{gb}). Table 2 presents R_b and R_{gb} values obtained by fitting curves depicted in Fig. 7 for all of the materials under study.

The results obtained for all of the compounds are in agreement with the internal barrier layer capacitance (IBLC) model proposed by Sinclair et al. [37] to explain the giant dielectric phenomenon of this ceramic. Both resistances R_b and R_{gb} increase for all doped ceramics compared to those of pure CCTO. In particular, the large increase of R_{gb} for samples doped with ZrO and n-ZrO_2 can be directly related to the lower values of tan(δ) since higher resistance of the barrier layer corresponds to lower conductance. Higher values of R_{gb} for Zr-doped samples could explain that the sample-electrode effect observed at low frequency for undoped CCTO is not present in doped ceramics as was proposed by Li et al. [38].

In the context of the IBLC model, the presence of high resistance grain boundaries and semiconducting grains is important to achieve superior dielectric properties. The frequency dependence of the loss tangent can be described using the equation [39]:

$$tan(\delta) = \frac{1}{\omega R_{gb} C_P} + \omega R_b C_P \quad (1)$$

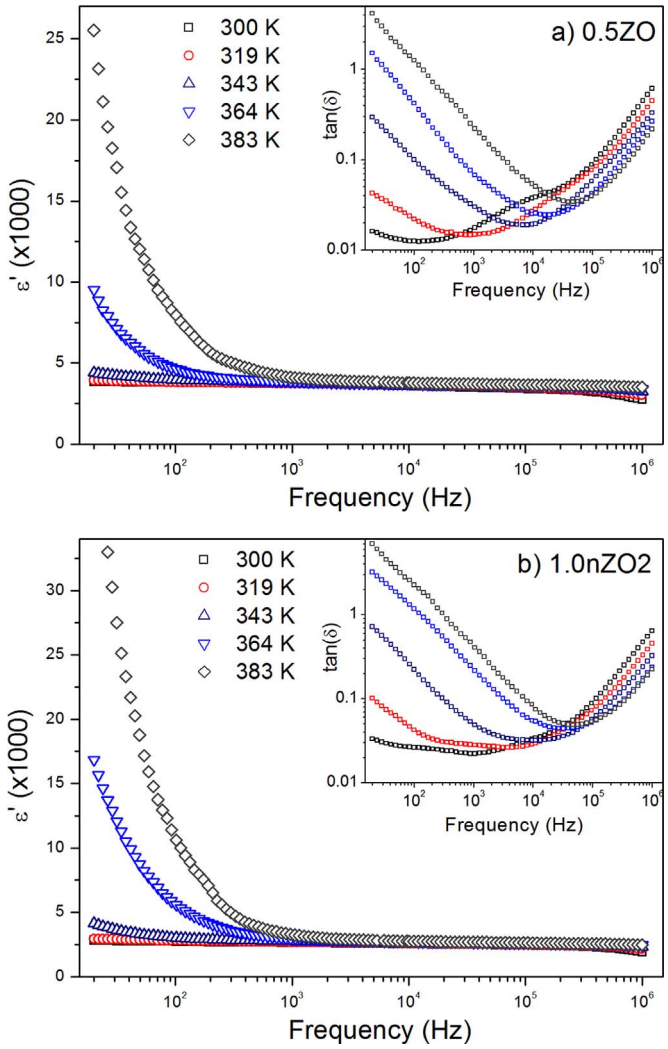

Fig. 8. Temperature dependence of dielectric constant (ε') and loss (tan(δ)) for samples (a) 0.5ZO and (b) 1.0nZO2.

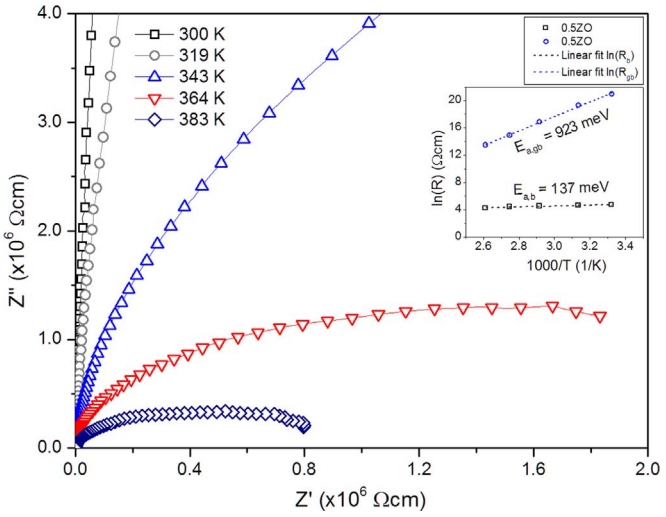

Fig. 9. Complex impedance plots at different temperatures for sample 0.5ZO. (inset) Temperature dependence of R_b and R_{gb}.

where ω is the angular frequency and C_P is the effective capacitance of the system. At low frequencies, the first term on the right side of Eq. (1) is important, and at frequencies over approximately 10 kHz, the second term becomes dominant. Eq. (1) qualitatively agrees with the results shown in Fig. 6(c) and (d), where in the low frequency regime the lowest tan(δ) values were obtained for the samples with higher R_{gb}.

The temperature dependence of dielectric properties for samples 0.5ZO and 1.0nZO2 is presented in Fig. 8(a) and (b), respectively. Both samples exhibited an almost frequency independent ε' until reaching 343 K, which at higher temperatures showed a strong increase at frequencies lower than 1 kHz. This is attributed to the sample-electrode interface effect that was observed in undoped CCTO at room temperature. Similar behavior was presented by the other doped samples. Additionally, evolution of the dielectric loss of samples 0.5ZO and 1.0ZO2 at different temperatures showed a displacement of the minimum tan(δ) value to higher frequencies with the increase in temperature, as is shown in the inset plots of Fig. 8(a) and (b). The shift of these relaxation curves as a function of temperature indicates that the electrical response is thermally activated, which can be measured by the impedance plots at different temperatures.

For all Zr-doped and pure CCTO samples, complex impedance plots evolved from bigger to lower semicircular arcs as the temperature increases, as can be seen for sample 0.5ZO in Fig. 9. This implies decreasing R_b and R_{gb} values as shown in the inset graph of Fig. 9. Activation energies can be calculated from the straight line slopes assuming an Arrhenius temperature dependence [14,24,28]. The obtained values are listed in Table 2 and are closed to activation energies reported for grains (100 meV) and grain boundaries (500–660 meV) in CCTO [37]. These higher energy values have been related to oxygen vacancies in the grain boundaries of CCTO compounds [14].

Characterization of the initial ZrO dopant by Rietveld refinement of the XRD pattern indicated that it was a non-stoichiometric compound instead of the cubic structure reported for ZrO in ICDD card 20-684 [40]. These structural oxygen defects of ZrO dopant would suppress the formation of oxygen vacancies at grain boundaries during thermal treatments leading to higher R_{gb} in ZrO-doped CCTO compared to that for m-ZrO_2 doping. This was also suggested by Chi et al. [22] as the mechanism responsible for the reduction of the dielectric loss and dielectric constant in Zr-doped CCTO.

Conversely, the influence of monoclinic ZrO_2 reported by Patterson et al. [18] is greatly improved by the reduction in size of n-ZrO_2. In this case, the effect of the dopant is enhanced by the higher surface area of the nanometric particles, which is evident by the increase in the activation energy at the higher dopant concentration. These results suggest that zirconium oxide-doping modifies the defect equilibrium of oxygen vacancies during the thermal treatments of the manufacturing process, suppressing the oxygen-loss from the bulk of grains and promoting the oxidation of the grain boundaries during cooling [22].

4. Conclusions

In summary, the improvements in the dielectric properties of the CCTO ceramic by ZrO_2 doping are enhanced by the use of non-stoichiometric Zr oxides and by a nanometric grain-size dopant. At a concentration of 0.5 wt%, the non-stoichiometric ZrO exhibits a higher dielectric constant and lower dissipation factor than that of ZrO_2, and similar results are obtained for nanometric ZrO_2 at a concentration of 1.0 wt%. These results provide new research opportunities for improving CCTO properties because the effect of stoichiometry and size of the dopant were not previously explored.

Acknowledgements

This work was funded by Fondecyt Project 1150652. The authors would like to thank Ramón Zárate for help with the impedance and Raman measurements and project EQU-33.

References

[1] M.A. Subramanian, D. Li, N. Duan, B.A. Reisner, A.W. Sleight, High dielectric constant in $ACu_3Ti_4O_{12}$ and $ACu_3Ti_3FeO_{12}$ phases, J. Solid State Chem. 151 (2000) 323–325. http://dx.doi.org/10.1006/jssc.2000.8703.

[2] A.P. Ramirez, M.A. Subramanian, M. Gardela, G. Blumberga, D. Li, T. Vogt, S.M. Shapiro, Giant dielectric constant response in a copper-titanate, Solid State Commun. 115 (2000) 217–220. http://dx.doi.org/10.1016/S0038-1098(00)00182-4.

[3] M.A. Subramanian, A.W. Sleight, $ACu_3Ti_4O_{12}$ and $ACu_3Ru_4O_{12}$ perovskites: high dielectric constants and valence degeneracy, Solid State Sci. 4 (2002) 347–351.

[4] S. Manik, S. Pradhan, Microstructure characterization of ball-mill-prepared nanocrystalline $CaCu_3Ti_4O_{12}$ by Rietveld method, Phys. E Low-Dimens. Syst. Nanostruct. 33 (2006) 160–168. http://dx.doi.org/10.1016/j.physe.2006.01.010.

[5] L. Wu, Y. Zhu, S. Park, S. Shapiro, G. Shirane, J. Tafto, Defect structure of the high-dielectric-constant perovskite $CaCu_3Ti_4O_{12}$, Phys. Rev. B 71 (2005). http://dx.doi.org/10.1103/PhysRevB.71.014118.

[6] P. Leret, J.F. Fernandez, J. de Frutos, D. Fernández-Hevia, Nonlinear I–V electrical behaviour of doped $CaCu_3Ti_4O_{12}$ ceramics, J. Eur. Ceram. Soc. 27 (2007) 3901–3905. http://dx.doi.org/10.1016/j.jeurceramsoc.2007.02.059.

[7] G. Chiodelli, V. Massarotti, D. Capsoni, M. Bini, C. Azzoni, M. Mozzati, P. Lupotto, Electric and dielectric properties of pure and doped CaCuTiO perovskite materials, Solid State Commun. 132 (2004) 241–246. http://dx.doi.org/10.1016/j.ssc.2004.07.058.

[8] D. Capsoni, M. Bini, V. Massarotti, G. Chiodelli, M.C. Mozzatic, C.B. Azzoni, Role of doping and CuO segregation in improving the giant permittivity of $CaCu_3Ti_4O_{12}$, J. Solid State Chem. 177 (2004) 4494–4500. http://dx.doi.org/10.1016/j.jssc.2004.09.009.

[9] A.K. Rai, K.D. Mandal, D. Kumar, O. Parkash, Characterization of nickel doped CCTO: $CaCu_{2.9}Ni_{0.1}Ti_4O_{12}$ and $CaCu_3Ti_{3.9}Ni_{0.1}O_{12}$ synthesized by semi-wet route, J. Alloy. Compd. 491 (2010) 507–512. http://dx.doi.org/10.1016/j.jallcom.2009.10.247.

[10] M. Li, A. Feteira, D.C. Sinclair, A.R. West, Influence of Mn doping on the semiconducting properties of $CaCu_3Ti_4O_{12}$ ceramics, Appl. Phys. Lett. 88 (2006) 232903. http://dx.doi.org/10.1063/1.2200732.

[11] B. Rivas-Murias, M. Sánchez-Andújar, J. Rivas, M.A. Señarís-Rodríguez, Influence of high levels of Nb and Ti doping on the dielectric properties of $CaCu_3Ti_4O_{12}$ type of compounds, Mater. Chem. Phys. 120 (2010) 576–581. http://dx.doi.org/10.1016/j.matchemphys.2009.12.006.

[12] M.A. Sulaiman, S.D. Hutagalung, J.J. Mohamed, Z.A. Ahmad, M.F. Ain, B. Ismail, High frequency response to the impedance complex properties of Nb-doped $CaCu_3Ti_4O_{12}$ electroceramics, J. Alloy. Compd. 509 (2011) 5701–5707. http://dx.doi.org/10.1016/j.jallcom.2011.02.145.

[13] A.K. Rai, K.D. Mandal, D. Kumar, O. Parkash, Dielectric properties of $CaCu_3Ti_{4-x}Co_xO_{12}$ (x=0.10, 0.20, and 0.30) synthesized by semi-wet route, Mater. Chem. Phys. 122 (2010) 217–223. http://dx.doi.org/10.1016/j.matchemphys.2010.02.037.

[14] Q. Zheng, H. Fan, C. Long, Microstructures and electrical responses of pure and chromium-doped $CaCu_3Ti_4O_{12}$ ceramics, J. Alloy. Compd. 511 (2012) 90–94. http://dx.doi.org/10.1016/j.jallcom.2011.09.002.

[15] L. Liu, Y. Huang, Y. Li, D. Shi, S. Zheng, S. Wu, L. Fang, C. Hu, Dielectric and non-Ohmic properties of $CaCu_3Ti_4O_{12}$ ceramics modified with NiO, SnO_2, SiO_2, and Al_2O_3 additives, J. Mater. Sci. 47 (2011) 2294–2299. http://dx.doi.org/10.1007/s10853-011-6043-1.

[16] T. Li, J. Chen, D. Liu, Z. Zhang, Z. Chen, Z. Li, X. Cao, B. Wang, Effect of NiO-

doping on the microstructure and the dielectric properties of $CaCu_3Ti_4O_{12}$ ceramics, Ceram. Int. (2014). http://dx.doi.org/10.1016/j.ceramint.2014.01.119.
[17] S. Vangchangyia, T. Yamwong, E. Swatsitang, P. Thongbai, S. Maensiri, Selectivity of doping ions to effectively improve dielectric and non-ohmic properties of $CaCu_3Ti_4O_{12}$ ceramics, Ceram. Int. 39 (2013) 8133–8139. http://dx.doi.org/10.1016/j.ceramint.2013.03.086.
[18] E.A. Patterson, S. Kwon, C.-C. Huang, D.P. Cann, Effects of ZrO_2 additions on the dielectric properties of $CaCu_3Ti_4O_{12}$, Appl. Phys. Lett. 87 (2005) 182911. http://dx.doi.org/10.1063/1.2126142.
[19] S. Jesurani, S. Kanagesan, M. Hashim, I. Ismail, Dielectric properties of Zr doped $CaCu_3Ti_4O_{12}$ synthesized by sol–gel route, J. Alloy. Compd. 551 (2013) 456–462. http://dx.doi.org/10.1016/j.jallcom.2012.11.043.
[20] S. Kwon, C.-C. Huang, E.A. Patterson, D.P. Cann, E.F. Alberta, S. Kwon, W.S. Hackenberger, The effect of Cr_2O_3, Nb_2O_5 and ZrO_2 doping on the dielectric properties of $CaCu_3Ti_4O_{12}$, Mater. Lett. 62 (2008) 633–636. http://dx.doi.org/10.1016/j.matlet.2007.06.042.
[21] L. Zhang, Y. Wu, X. Guo, Z. Wang, Y. Zou, Influence of Zr doping on the dielectric properties of $CaCu_3Ti_4O_{12}$ ceramics, J. Mater. Sci. Mater. Electron. 23 (2011) 865–869. http://dx.doi.org/10.1007/s10854-011-0508-5.
[22] Q.G. Chi, L. Gao, X. Wang, J.Q. Lin, J. Sun, Q.Q. Lei, Effects of Zr doping on the microstructures and dielectric properties of $CaCu_3Ti_4O_{12}$ ceramics, J. Alloy. Compd. 559 (2013) 45–48. http://dx.doi.org/10.1016/j.jallcom.2013.01.090.
[23] L. Sun, Z. Wang, W. Hao, E. Cao, Y. Zhang, H. Peng, Influence of zirconium doping on microstructure and dielectric properties of $CaCu_3Ti_4O_{12}$ synthesized by the sol–gel method, J. Alloy. Compd. 651 (2015) 283–289. http://dx.doi.org/10.1016/j.jallcom.2015.08.111.
[24] P. Thongbai, J. Jumpatam, B. Putasaeng, T. Yamwong, S. Maensiri, Microstructural evolution and Maxwell-Wagner relaxation in $Ca_2Cu_2Ti_{4-x}Zr_xO_{12}$: the important clue to achieve the origin of the giant dielectric behavior, Mater. Res. Bull. 60 (2015) 695–703. http://dx.doi.org/10.1016/j.materresbull.2014.09.045.
[25] S.D. Hutagalung, L.Y. Ooi, Z.A. Ahmad, Improvement in dielectric properties of Zn-doped $CaCu_3Ti_4O_{12}$ electroceramics prepared by modified mechanical alloying technique, J. Alloy. Compd. 476 (2009) 477–481. http://dx.doi.org/10.1016/j.jallcom.2008.09.025.
[26] L. Singh, U.S. Rai, K.D. Mandal, Dielectric properties of zinc doped nanocrystalline calcium copper titanate synthesized by different approach, Mater. Res. Bull. 48 (2013) 2117–2122. http://dx.doi.org/10.1016/j.materresbull.2013.02.005.
[27] H. Yu, H. Liu, H. Hao, D. Luo, M. Cao, Dielectric properties of CaCu3Ti4O12 ceramics modified by SrTiO3, Mater. Lett. 62 (2008) 1353–1355. http://dx.doi.org/10.1016/j.matlet.2007.08.052.
[28] C.-H. Mu, P. Liu, Y. He, J.-P. Zhou, H.-W. Zhang, An effective method to decrease dielectric loss of $CaCu_3Ti_4O_{12}$ ceramics, J. Alloy. Compd. 471 (2009) 137–141. http://dx.doi.org/10.1016/j.jallcom.2008.04.040.
[29] H. Xue, X. Guan, R. Yu, Z. Xiong, Dielectric properties and current–voltage nonlinear behavior of $Ca_{1-x}Sr_xCu_3Ti_4O_{12}$ ceramics, J. Alloy. Compd. 482 (2009) L14–L17. http://dx.doi.org/10.1016/j.jallcom.2009.03.190.
[30] K. Meeporn, T. Yamwong, S. Pinitsoontorn, V. Amornkitbamrung, P. Thongbai, Grain size independence of giant dielectric permittivity of $CaCu_3Ti_{4-x}Sc_xO_{12}$ ceramics, Ceram. Int. 40 (2014) 15897–15906. http://dx.doi.org/10.1016/j.ceramint.2014.07.118.
[31] A.K. Thomas, K. Abraham, J. Thomas, K.V. Saban, Structural and dielectric properties of A- and B-sites doped $CaCu_3Ti_4O_{12}$ ceramics, Ceram. Int. 41 (2015) 10250–10255. http://dx.doi.org/10.1016/j.ceramint.2015.04.138.
[32] J. Boonlakhorn, B. Putasaeng, P. Kidkhunthod, P. Thongbai, Improved dielectric properties of (Y + Mg) co-doped $CaCu_3Ti_4O_{12}$ ceramics by controlling geometric and intrinsic properties of grain boundaries, Mater. Des. 92 (2016) 494–498. http://dx.doi.org/10.1016/j.matdes.2015.12.042.
[33] Y. Su, W. Zhang, Dielectric properties and electrical conductivity of $CaCu_3Ti_4O_{12}$ ceramics doped with Zr4+, J. Wuhan Univ. Technol. Sci. Ed. 28 (2013) 343–346. http://dx.doi.org/10.1007/s11595-013-0691-8.
[34] W.L. Li, Y. Zhao, Q.G. Chi, Z.G. Zhang, W.D. Fei, Enhanced performance of core-shell-like structure Zr-doped $CaCu_3Ti_4O_{12}$ ceramics prepared by a flame synthetic approach, RSC Adv. (2012) 6073–6078. http://dx.doi.org/10.1039/c2ra20806g.
[35] J.J. Romero, P. Leret, F. Rubio-Marcos, A. Quesada, J.F. Fernández, Evolution of the intergranular phase during sintering of $CaCu_3Ti_4O_{12}$ ceramics, J. Eur. Ceram. Soc. 30 (2010) 737–742. http://dx.doi.org/10.1016/j.jeurceramsoc.2009.08.024.
[36] N. Kolev, R. Bontchev, A. Jacobson, V. Popov, V. Hadjiev, A. Litvinchuk, M. Iliev, Raman spectroscopy of $CaCu_3Ti_4O_{12}$, Phys. Rev. B 66 (2002). http://dx.doi.org/10.1103/PhysRevB.66.132102.
[37] T. Adams, D. Sinclair, A. West, Characterization of grain boundary impedances in fine- and coarse-grained $CaCu_3Ti_4O_{12}$ ceramics, Phys. Rev. B 73 (2006). http://dx.doi.org/10.1103/PhysRevB.73.094124.
[38] M. Li, D.C. Sinclair, A.R. West, Extrinsic origins of the apparent relaxorlike behavior in $CaCu_3Ti_4O_{12}$ ceramics at high temperatures: a cautionary tale, J. Appl. Phys. 109 (2011) 84106. http://dx.doi.org/10.1063/1.3572256.
[39] L. Feng, X. Tang, Y. Yan, X. Chen, Z. Jiao, G. Cao, Decrease of dielectric loss in $CaCu_3Ti_4O_{12}$ ceramics by La doping, Phys. Status Solidi 203 (2006) R22–R24. http://dx.doi.org/10.1002/pssa.200622038.
[40] R. Espinoza-González, E. Mosquera, Í. Moglia, R. Villarroel, V.M. Fuenzalida, Hydrothermal growth and characterization of zirconia nanostructures on non-stoichiometric zirconium oxide, Ceram. Int. 40 (2014). http://dx.doi.org/10.1016/j.ceramint.2014.07.034.